Robotica (2016) volume 34, pp. 1367–1382. © Cambridge University Press 2014
doi:10.1017/S0263574714002343

Saturated control of flexible-joint manipulators using a Hammerstein strictly positive real compensator

Ryan James Caverly*, David Evan Zlotnik and James Richard Forbes

Department of Aerospace Engineering, University of Michigan, Ann Arbor, MI, USA

(Accepted August 11, 2014. First published online: September 10, 2014)

SUMMARY

In this paper the control of flexible-joint manipulators while explicitly avoiding actuator saturation is considered. The controllers investigated are composed of a bounded proportional control term and a Hammerstein strictly positive real angular rate control term. This control structure ensures that the total torque demanded of each actuator is bounded by a value that is less than the maximum torque that each actuator is able to provide, thereby disallowing actuator saturation. The proposed controllers are shown to render the closed-loop system asymptotically stable, even in the presence of modeling uncertainties. The performance of the controllers is demonstrated experimentally and in simulation.

KEYWORDS: Control of robotic systems; Actuator saturation; Flexible-joint manipulators; Gibbs parameter; Serial manipulator; SPR compensator.

1. Introduction

The control of flexible-joint manipulators is a problem that has been identified and studied thoroughly. It has been shown that the unmodeled flexibility of manipulator joints can cause the manipulator to exhibit reduced performance and even become unstable.[1] This flexibility is most often caused by the belts, chains, torsional shafts, gear reducers, harmonic drives, etc., that actuate the manipulator's joints.[2] Many authors have developed dynamic models for joint flexibility,[3–8] and some have addressed the control of flexible-joint manipulators explicitly.[3–5,8–14] The control techniques considered include passivity-based control,[3,9] proportional-derivative (PD) control,[5,8] backstepping control,[10] adaptive control,[4,11] and neuroadaptive control.[13]

Actuator saturation is a prevalent issue that must be accounted for when controlling flexible-joint manipulators. The actuators on board a manipulator can only provide a finite amount of torque, which may be less than the torque demanded by the controller. Even a well-designed system could encounter actuator saturation in the presence of large, unexpected disturbances.[15] As such, it is highly desirable to design a control architecture that explicitly accounts for actuator saturation, while simultaneously guaranteeing stability of the closed-loop system. The control laws presented in ref. [6,8,10,16–19] are designed to avoid actuator saturation when controlling robotic manipulators using several different bounded functions. In particular, ref. [8] presents a PD control law that avoids actuator saturation by means of bounded saturation functions.

The control law presented in this paper uses a proportional control term found in ref. [8] involving a Gibbs parameterization of the joint angles, and a dynamic nonlinear derivative control term with an input nonlinearity inspired by refs. [20,21]. The use of Gibbs parameters instead of Euler angles is motivated by an increase in proportional control effort further away from the desired set point and an increased region of attraction when examining the stability of the closed-loop system in Section 4.2. The dynamic derivative control term is synthesized to be a strictly positive real (SPR) system using a method outlined in ref. [22], which allows the derivative control to be tuned over a bandwidth, giving

* Corresponding author. E-mail: caverly@umich.edu

https://doi.org/10.1017/S0263574714002343 Published online by Cambridge University Press

the ability to filter out measurement noise. The avoidance of actuator saturation is accomplished by the bounded nature of the proportional control term and by introducing a nonlinear input to the SPR derivative controller, thus creating a Hammerstein SPR derivative controller. Although the components of the proposed controller have all been previously used independently for different applications, the novel contribution of this paper is the combined use of a Hammerstein SPR derivative controller and a bounded proportional controller based on the Gibbs parameter to control flexible-joint manipulators. This control structure is proven to render the closed-loop system asymptotically stable, while simultaneously guaranteeing that actuator saturation is avoided.

The paper will proceed as follows. The system dynamics of a multi-link flexible-joint robotic manipulator are first reviewed. The proposed control law is then presented, including the structure of the proportional control term and the dynamic nonlinear derivative term. The asymptotic stability of the closed-loop system is proven and shown to be robust to modeling errors. The controllers are then tested experimentally on a single-link flexible-joint testbed, in order to demonstrate their performance. Finally, the controllers are tested in a numerical simulation of a two-link flexible-joint manipulator.

2. Preliminaries

2.1. Gibbs parameter

Consider the Gibbs parameter, $\bar{\mathbf{p}} \in \mathbb{R}^3$, that is defined as[23]

$$\bar{\mathbf{p}} = \bar{\mathbf{a}} \tan(\theta/2), \tag{1}$$

where $\bar{\mathbf{a}}$ is the axis of rotation and θ is the angle of rotation about the axis. The relationship between the angular velocity, $\bar{\boldsymbol{\omega}}$, and the time rate of change of the Gibbs parameter is

$$\dot{\bar{\mathbf{p}}} = \frac{1}{2}\left(\mathbf{1} + \bar{\mathbf{p}}^{\times} + \bar{\mathbf{p}}\bar{\mathbf{p}}^{\mathrm{T}}\right)\bar{\boldsymbol{\omega}}, \tag{2}$$

where

$$\bar{\mathbf{p}}^{\times} = \begin{bmatrix} 0 & -p_3 & p_2 \\ p_3 & 0 & -p_1 \\ -p_2 & p_1 & 0 \end{bmatrix} \tag{3}$$

is a skew-symmetric matrix satisfying $\bar{\mathbf{p}}^{\times^{\mathrm{T}}} = -\bar{\mathbf{p}}^{\times}\ \forall \bar{\mathbf{p}} \in \mathbb{R}^3$, $\bar{\mathbf{p}} = [p_1 \quad p_2 \quad p_3]^{\mathrm{T}}$. Considering only rotation about a single axis, Eqs. (1) and (2) simplify to

$$p = \tan(\theta/2), \tag{4}$$

$$\dot{p} = \frac{1}{2}\left(1 + p^2\right)\omega. \tag{5}$$

2.2. Strictly positive real system

Lemma 1 (*Kalman-Yakubovich-Popov (KYP) Lemma*[24]). Consider the linear time-invariant (LTI) system

$$\dot{\mathbf{x}}_c = \mathbf{A}_c\mathbf{x}_c + \mathbf{B}_c\mathbf{u}_c \tag{6}$$

$$\mathbf{y}_c = \mathbf{C}_c\mathbf{x}_c, \tag{7}$$

where $\mathbf{x}_c \in \mathbb{R}^n$, $\mathbf{u}_c, \mathbf{y}_c \in \mathbb{R}^m$, the constant matrices are defined as $\mathbf{A}_c \in \mathbb{R}^{n\times n}$, $\mathbf{B}_c \in \mathbb{R}^{n\times m}$, and $\mathbf{C}_c \in \mathbb{R}^{m\times n}$, and ($\mathbf{A}_c$,$\mathbf{B}_c$,$\mathbf{C}_c$) is a minimal state-space realization. The system is SPR if and only if there exists $\mathbf{P}_c \in \mathbb{R}^{n\times n}$ and $\mathbf{Q}_c \in \mathbb{R}^{n\times n}$, where $\mathbf{P}_c = \mathbf{P}_c^{\mathrm{T}} > 0$ and $\mathbf{Q}_c = \mathbf{Q}_c^{\mathrm{T}} > 0$ such that the following

https://doi.org/10.1017/S0263574714002343 Published online by Cambridge University Press

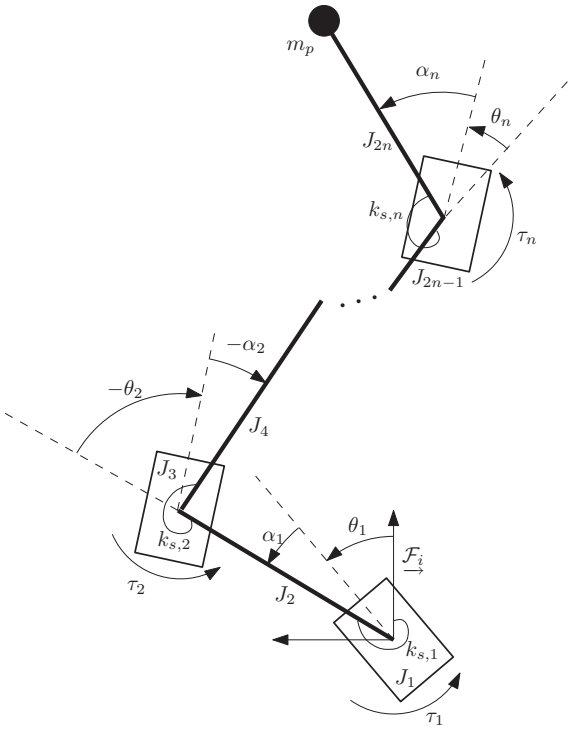


Fig. 1. Schematic of a multi-link flexible-joint robotic manipulator.

equations are satisfied:

$$\mathbf{P}_c\mathbf{A}_c + \mathbf{A}_c^{\mathrm{T}}\mathbf{P}_c = -\mathbf{Q}_c \tag{8}$$

$$\mathbf{P}_c\mathbf{B}_c = \mathbf{C}_c^{\mathrm{T}}. \tag{9}$$

3. System Dynamics

The equations of motion of a multi-link flexible-joint manipulator, shown in Fig. 1 can be modeled as[3–7]

$$\mathbf{M}(\mathbf{q}, \dot{\mathbf{q}})\ddot{\mathbf{q}} + \mathbf{D}\dot{\mathbf{q}} + \mathbf{K}\mathbf{q} = \hat{\mathbf{B}}\boldsymbol{\tau} + \mathbf{f}_{\mathrm{non}}, \tag{10}$$

where $\mathbf{M} = \mathbf{M}^{\mathrm{T}} > 0$ is the system's mass matrix, $\mathbf{D} = \mathbf{D}^{\mathrm{T}} \geq 0$ is the system's damping matrix, $\mathbf{K} = \mathbf{K}^{\mathrm{T}} \geq 0$ is the system's stiffness matrix, $\hat{\mathbf{B}} = [\mathbf{1} \quad \mathbf{0}]^{\mathrm{T}}$ is the column vector that distributes the applied torques to the system, $\boldsymbol{\tau} = [\tau_1 \quad \tau_2 \quad \cdots \quad \tau_n]^{\mathrm{T}}$ is the column vector of torque inputs to the system, $\mathbf{f}_{\mathrm{non}} = -\mathbf{C}(\mathbf{q}, \dot{\mathbf{q}})\dot{\mathbf{q}}$ is the column vector of nonlinear forces, $\mathbf{C}(\mathbf{q}, \dot{\mathbf{q}})$ is a matrix function of $\mathbf{q}$ and $\dot{\mathbf{q}}$, $\mathbf{q} = [\theta_1 \quad \theta_2 \quad \cdots \quad \theta_n \quad \alpha_1 \quad \alpha_2 \quad \cdots \quad \alpha_n]^{\mathrm{T}}$ are the generalized coordinates of the system, and $\mathbf{1}$ is the identity matrix of appropriate dimension. The angle $\theta_i,\ i = 1, 2, \ldots, n$ is the joint angle of the i^{th} hub with respect to the previous link and the angle $\alpha_i,\ i = 1, 2, \ldots, n$ is the angle of the i^{th} link with respect to the i^{th} hub. The subscript i denotes the properties of the i^{th} hub and link. Gravitational forces have been neglected in this model, but could be accounted for by implementing a feedforward control term as described in ref. [3]. Note that for serial manipulators the matrix $(\dot{\mathbf{M}} - 2\mathbf{C})$ is skew-symmetric.[25] Moreover, the total energy of this system is $E = \frac{1}{2}\dot{\mathbf{q}}^{\mathrm{T}}\mathbf{M}\dot{\mathbf{q}} + \frac{1}{2}\mathbf{q}^{\mathrm{T}}\mathbf{K}\mathbf{q}$ and the time derivative of the total energy is $\dot{E} = \dot{\mathbf{q}}^{\mathrm{T}}\mathbf{D}\dot{\mathbf{q}} + \dot{\mathbf{q}}^{\mathrm{T}}\hat{\mathbf{B}}\boldsymbol{\tau}_c$.

In Fig. 1, $k_{s,i}$ is the stiffness of the i^{th} flexible joint, J_{2i-1} is the second moment of mass of the i^{th} hub, J_{2i} is the second moment of mass of the i^{th} link, and m_p is the mass of the payload.

https://doi.org/10.1017/S0263574714002343 Published online by Cambridge University Press

4. Control Formulation

4.1. Control law

Consider the following PD control law:

$$\boldsymbol{\tau} = \mathbf{u}_p + \mathbf{u}_d, \tag{11}$$

where $\mathbf{u}_p = [u_{p,1} \quad u_{p,2} \quad \cdots \quad u_{p,n}]^{\mathrm{T}}$ is proportional control and $\mathbf{u}_d = [u_{d,1} \quad u_{d,2} \quad \cdots \quad u_{d,n}]^{\mathrm{T}}$ is derivative control. Actuator saturation can be avoided if the total torque demanded from each of the manipulator's actuators is bounded by a value lower than the maximum torque that each actuator can provide. Proportional and derivative control functions of $u_{p,i} = -k_{ps,i} \frac{k_{p,i} p_i}{\sqrt{1+k_{p,i}^2 p_i^2}}$ or $u_{p,i} = -k_{ps,i} \frac{k_{p,i} \theta_i / 2}{\sqrt{1+k_{p,i}^2 \theta_i^2 / 4}}$, and $u_{d,i} = -k_{ds,i} \frac{k_{d,i} \omega_i}{\sqrt{1+k_{d,i}^2 \omega_i^2}}$ are used in ref. [8], where $p_i = \tan(\theta_i/2)$ is a Gibbs parametrization of the i^{th} joint angle, and $\omega_i = \dot{\theta}_i$ is the i^{th} joint rate. This control architecture guarantees $|\tau_i| \leq k_{p,i} + k_{d,i}, \ \ i = 1, 2, \ldots, n$. Provided that the control gains $k_{p,i}$ and $k_{d,i}$ are chosen so that $k_{p,i} + k_{d,i} < \tau_{s,i}, \quad i = 1, 2, \ldots, n$, where $\tau_{s,i}$ is the saturation limit of the i^{th} actuator, the control torque demanded from each actuator will be less its saturation limit.

This paper uses the proportional control law in ref. [8] and introduces a dynamic compensator to be used for derivative control. This is motivated by the ability to tune a dynamic controller over a bandwidth, and as a result reject measurement noise. Consider the following control architecture:

$$\boldsymbol{\tau} = \mathbf{u}_p + \boldsymbol{\sigma}(\mathbf{u}), \tag{12}$$

where $\mathbf{u}$ is derivative control, $\boldsymbol{\sigma}$ is an input nonlinearity, and $\mathbf{u}_d = \boldsymbol{\sigma}(\mathbf{u}) = [\sigma_1(u_1) \ \sigma_2(u_2) \ \cdots \ \sigma_n(u_n)]^{\mathrm{T}}$ is nonlinear derivative control. In particular, $\sigma_i(\cdot)$ will account for saturation, and has the following form:

$$\sigma_i(u_i) = \begin{cases} u_i & |u_i| \leq \bar{u}_i \\ \text{sign}(u_i)\bar{u}_i & |u_i| > \bar{u}_i \end{cases}, \ i = 1, 2, \ldots, n, \tag{13}$$

where $\bar{u}_i$ is the user-defined derivative control saturation limit of the i^{th} actuator, $\text{sign}(u_i) = +1$ if $u_i > 0$, $\text{sign}(u_i) = 0$ if $u_i = 0$, and $\text{sign}(u_i) = -1$ if $u_i < 0$. The derivative control saturation limit of the i^{th} actuator, $\bar{u}_i$, is chosen so that $k_{p,i} + \bar{u}_i < \tau_{s,i}$. The nonlinearity $\boldsymbol{\beta}$ is defined as[20]

$$\boldsymbol{\beta}(\mathbf{u})\mathbf{u} = \boldsymbol{\sigma}(\mathbf{u}), \tag{14}$$

where $\boldsymbol{\beta} = \text{diag}\{\beta_1(u_1), \beta_2(u_2), \ldots, \beta_n(u_n)\}$ and

$$\beta_i(u_i) = \begin{cases} \sigma_i(u_i)/u_i & u_i \neq 0 \\ \xi_i & u_i = 0 \end{cases}, \ i = 1, 2, \ldots, n, \tag{15}$$

while ξ_i is chosen arbitrarily to ensure that $\beta_i(u_i)$ is defined when $u_i = 0$. In this paper $\xi_i = 1, \ i = 1, 2, \ldots, n$.

The derivative control term of Eq. (12) will be the output of a SPR system with input $\mathbf{u}_c = \hat{\mathbf{y}} = \boldsymbol{\beta}(\mathbf{u})\boldsymbol{\omega}$:

$$\dot{\mathbf{x}}_c = \mathbf{A}_c\mathbf{x}_c + \mathbf{B}_c\mathbf{u}_c \tag{16}$$

$$-\mathbf{u} = \mathbf{y}_c = \mathbf{C}_c\mathbf{x}_c, \tag{17}$$

where $\boldsymbol{\omega} = [\omega_1 \ \ \omega_2 \ \ \cdots \ \ \omega_n]^{\mathrm{T}}$. This controller is a Hammerstein SPR system, which is inspired by the controllers presented in ref. [20, 21]. A Hammerstein system is a linear system with an input nonlinearity.

The proportional control term will use the saturation function from ref. [8] with either Gibbs parameters or the joint angles directly:

$$\mathbf{u}_p = -\mathbf{K}_p\mathbf{f}(\mathbf{p}) \tag{18}$$

https://doi.org/10.1017/S0263574714002343 Published online by Cambridge University Press

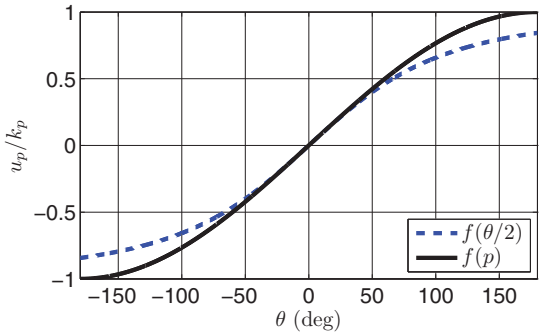


Fig. 2. Relative control effort vs. θ. The function $f(p)$ provides more relative control effort than $f(\theta/2)$ as θ approaches 180°, which motivates the use of the Gibbs parameter.

or

$$\mathbf{u}_p = -\mathbf{K}_p \mathbf{f}(\boldsymbol{\theta}/2), \tag{19}$$

where $\mathbf{K}_p = \text{diag}\{k_{p,1}, k_{p,2}, \ldots, k_{p,n}\}$, $\mathbf{p} = [p_1 \quad p_2 \quad \cdots \quad p_n]^{\mathrm{T}}$, $\boldsymbol{\theta} = [\theta_1 \quad \theta_2 \quad \cdots \quad \theta_n]^{\mathrm{T}}$, $\mathbf{f}(\mathbf{p}) = [f(p_1) \quad f(p_2) \quad \cdots \quad f(p_n)]^{\mathrm{T}}$, $\mathbf{f}(\boldsymbol{\theta}) = [f(\theta_1) \quad f(\theta_2) \quad \cdots \quad f(\theta_n)]^{\mathrm{T}}$, $f(x) = x/\sqrt{1+x^2}$, and $0 < k_{p,i} < \infty$, $i = 1, \ldots, n$. It is worth noting that the function $f(p)$ is equivalent to $\sin(\theta/2)$ on the interval $-\pi \leq \theta \leq \pi$.

The following proposed control laws are investigated:

$$\boldsymbol{\tau} = -\mathbf{K}_p \mathbf{f}(\mathbf{p}) + \boldsymbol{\sigma}(\mathbf{u}), \tag{20}$$

$$\boldsymbol{\tau} = -\mathbf{K}_p \mathbf{f}(\boldsymbol{\theta}/2) + \boldsymbol{\sigma}(\mathbf{u}). \tag{21}$$

The angle $\theta/2$ is used to match the linearization of $p = \tan(\theta/2)$ about $\theta = 0°$, and is included in the control law for the purpose of comparing the use of Euler angles to Gibbs parameters. A comparison of the relative control effort supplied by the functions $f(p)$ and $f(\theta/2)$ is presented in Fig. 2.

The function $f(p)$ is shown to provide more relative control effort than the function $f(\theta/2)$ as the angle increases. This serves as motivation to use the function $f(p)$ in the control architecture. Additionally, actuator saturation tends to occur when a large, quick maneuver is being performed, which corresponds to the region where $f(p)$ has a higher relative control effort. This could potentially allow both saturation functions to avoid saturation differently.

Note that the control law in Eq. (12) is somewhat conservative, as the proportional control and nonlinear derivative control may not necessarily saturate simultaneously. If either the proportional or nonlinear derivative control term saturates individually, then the total control effort demanded will be bounded below the actuator's saturation limit and a certain amount of usable control effort may be wasted. Although this control law is conservative, it guarantees that $|\tau_i| \leq k_{p,i} + \bar{u}_i < \tau_{s,i}, \quad i = 1, 2, \ldots, n$, where $\tau_{s,i}$ is the saturation limit of the i^{th} actuator. Also, note that different saturation limits can be chosen for each individual actuator by choosing different values of $k_{p,i}$ and $\bar{u}_i$. Robotic manipulators typically have powerful motors at the base and significantly smaller, and thus weaker, motors towards the end effector, which can be accounted for in the proposed control architecture by decreasing the saturation limit in the smaller actuators. This will allow each individual actuator to approach its own saturation limit.

Block diagrams of the control laws proposed in Eqs. (20) and (21) are shown in Figs. 3 and 4.

4.2. Stability analysis

In the following proofs, a restriction is applied to the allowable set of initial conditions. The Gibbs parameter exhibits a singularity at $\theta_i = \pm\pi$, $i = 1, 2, \ldots, n$, and as such, these configurations should be avoided. As long as θ_i remains on the domain $-\pi < \theta_i < \pi$, the Gibbs parameter will not reach a singularity. When using the control law of Eq. (21) the angle θ_i, $i = 1, 2, \ldots, n$ could experience unwinding if it does not remain on the same domain $-\pi < \theta_i < \pi$. Unwinding occurs when a body is

https://doi.org/10.1017/S0263574714002343 Published online by Cambridge University Press

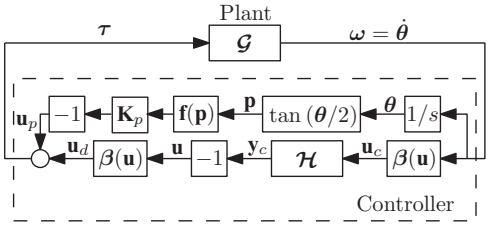


Fig. 3. Block diagram of the control law in Eq. (20), where $\mathcal{G}$ is the plant with dynamics defined by Eq. (10) and $\mathcal{H}$ is the controller defined in Eqs. (16) and (17).

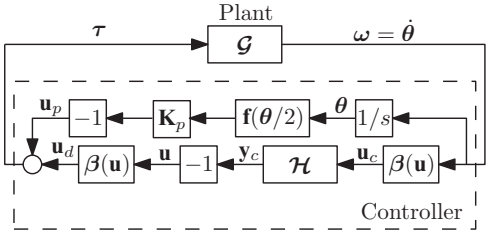


Fig. 4. Block diagram of the control law in Eq. (21), where $\mathcal{G}$ is the plant with dynamics defined by Eq. (10) and $\mathcal{H}$ is the controller defined in Eqs. (16) and (17).

relatively close to a desired set point, yet rotates through one or more full revolutions before settling at the desired set point.[27] To illustrate this phenomenon, consider the situation when the manipulator hub starts at an angle of $+359^\circ$, which is also -1°, and has zero initial angular velocity. Assuming that the desired set point is 0°, the controller would then drive the manipulator away from the zero degree position, all the way through $+180^\circ$, and eventually back to an attitude of 0°; clearly, this unwinding effect is not desirable. By restricting the set of allowable initial conditions, singularities will be avoided and unwinding will not occur. Restrictions on initial conditions have been used previously in ref. [28,29], in the context of spacecraft attitude control. In addition, it will be assumed that $\sqrt{\mathbf{D}}\dot{\mathbf{q}} = \mathbf{0}$ and $\dot{\boldsymbol{\theta}} = \hat{\mathbf{B}}^{\mathrm{T}}\dot{\mathbf{q}} = \mathbf{0}$ implies that $\dot{\mathbf{q}} = \mathbf{0}$. This is known as zero-rate detectability,[30] which is similar to the zero-state detectability hypothesis found in ref. [31]. Without loss of generality, it will be assumed that the desired set point is zero angular position and zero angular velocity of the manipulator. Other set points could be considered with trivial modification to the following proofs.

Theorem 1. The dynamics of the multi-link flexible-joint manipulator found in Eq. (10) on the domain $-\pi < \theta_i < \pi, -\pi < \alpha_i < \pi, \dot{\theta}_i \in \mathbb{R}, \dot{\alpha}_i \in \mathbb{R},\ i = 1, 2, \ldots, n$ together with the control law given by Eq. (20) render the equilibrium point $(\mathbf{q}, \dot{\mathbf{q}}, \mathbf{x}_c) = (\mathbf{0}, \mathbf{0}, \mathbf{0})$ of the closed-loop system asymptotically stable if

$$V_1(\mathbf{q}(0), \dot{\mathbf{q}}(0), \mathbf{x}_c(0)) = \frac{1}{2}\dot{\mathbf{q}}^{\mathrm{T}}(0)\mathbf{M}\dot{\mathbf{q}}(0) + \frac{1}{2}\mathbf{q}^{\mathrm{T}}(0)\mathbf{K}\mathbf{q}(0) + \frac{1}{2}\mathbf{x}_c^{\mathrm{T}}(0)\mathbf{P}_c\mathbf{x}_c(0) + \sum_{i=1}^{n} 2k_{p,i}\left(1 - \frac{1}{\sqrt{1 + p_i^2(0)}}\right) < \sum_{i=1}^{n} 2k_{p,i}. \tag{22}$$

Proof. First, note that it can be easily shown using Eq. (10) and Eq. (20) that $(\mathbf{q}, \dot{\mathbf{q}}, \mathbf{x}_c) = (\mathbf{0}, \mathbf{0}, \mathbf{0})$ is in fact an equilibrium point of the closed-loop system. Let

$$\boldsymbol{\tau} = \mathbf{u}_p + \boldsymbol{\sigma}(\mathbf{u}) = -\mathbf{K}_p \begin{bmatrix} f(p_1) \\ f(p_2) \\ \vdots \\ f(p_n) \end{bmatrix} + \boldsymbol{\sigma}(\mathbf{u}), \tag{23}$$

https://doi.org/10.1017/S0263574714002343 Published online by Cambridge University Press

where $f(p_i) = p_i/\sqrt{1+p_i^2},\ i = 1, 2, \ldots, n$. Now, consider the following Lyapunov function candidate,

$$V_1(\mathbf{q}, \dot{\mathbf{q}}, \mathbf{x}_c) = \frac{1}{2}\dot{\mathbf{q}}^{\mathrm{T}}\mathbf{M}\dot{\mathbf{q}} + \frac{1}{2}\mathbf{q}^{\mathrm{T}}\mathbf{K}\mathbf{q} + \sum_{i=1}^{n} 2k_{p,i}\left(1 - \frac{1}{\sqrt{1+p_i^2}}\right) + \frac{1}{2}\mathbf{x}_c^{\mathrm{T}}\mathbf{P}_c\mathbf{x}_c. \tag{24}$$

Taking the derivative of V_1 with respect to time and simplifying using Eqs. (10) and (5) gives

$$\dot{V}_1 = \dot{\mathbf{q}}^{\mathrm{T}}\left(\mathbf{M}\ddot{\mathbf{q}} + \frac{1}{2}\dot{\mathbf{M}}\dot{\mathbf{q}} + \mathbf{K}\mathbf{q}\right) + \sum_{i=1}^{n} k_{p,i}\frac{p_i(1+p_i^2)\omega_i}{(1+p_i^2)^{\frac{3}{2}}} + \frac{1}{2}\mathbf{x}_c^{\mathrm{T}}\left(\mathbf{P}_c\mathbf{A}_c + \mathbf{A}_c^{\mathrm{T}}\mathbf{P}_c\right)\mathbf{x}_c + \mathbf{x}_c^{\mathrm{T}}\mathbf{P}_c\mathbf{B}_c\hat{\mathbf{y}} \tag{25}$$

$$= \dot{\mathbf{q}}^{\mathrm{T}}(-\mathbf{D}\dot{\mathbf{q}} + \hat{\mathbf{b}}\boldsymbol{\tau}) + \sum_{i=1}^{n} k_{p,i}\frac{p_i\omega_i}{\sqrt{1+p_i^2}} - \frac{1}{2}\mathbf{x}_c^{\mathrm{T}}\mathbf{Q}_c\mathbf{x}_c + \mathbf{x}_c^{\mathrm{T}}\mathbf{C}_c^{\mathrm{T}}\hat{\mathbf{y}} \tag{26}$$

$$= \dot{\mathbf{q}}^{\mathrm{T}}\hat{\mathbf{b}}\left(-\mathbf{K}_p\begin{bmatrix} f(p_1) \\ f(p_2) \\ \vdots \\ f(p_n) \end{bmatrix} + \boldsymbol{\sigma}(\mathbf{u})\right) - \dot{\mathbf{q}}^{\mathrm{T}}\mathbf{D}\dot{\mathbf{q}} + \sum_{i=1}^{n} k_{p,i}\frac{p_i\omega_i}{\sqrt{1+p_i^2}} - \frac{1}{2}\mathbf{x}_c^{\mathrm{T}}\mathbf{Q}_c\mathbf{x}_c - \mathbf{u}^{\mathrm{T}}\hat{\mathbf{y}} \tag{27}$$

$$= -\dot{\mathbf{q}}^{\mathrm{T}}\mathbf{D}\dot{\mathbf{q}} + \boldsymbol{\omega}^{\mathrm{T}}\boldsymbol{\sigma}(\mathbf{u}) - \frac{1}{2}\mathbf{x}_c^{\mathrm{T}}\mathbf{Q}_c\mathbf{x}_c - \hat{\mathbf{y}}^{\mathrm{T}}\mathbf{u} \tag{28}$$

Substituting in the definitions $\boldsymbol{\omega}(\mathbf{u}) = \boldsymbol{\beta}(\mathbf{u})\mathbf{u}$ and $\hat{\mathbf{y}} = \boldsymbol{\beta}(\mathbf{u})\boldsymbol{\omega}$ into Eq. (28) yields

$$\dot{V}_1 = -\dot{\mathbf{q}}^{\mathrm{T}}\mathbf{D}\dot{\mathbf{q}} + \boldsymbol{\omega}^{\mathrm{T}}\boldsymbol{\beta}(\mathbf{u})\mathbf{u} - \frac{1}{2}\mathbf{x}_c^{\mathrm{T}}\mathbf{Q}_c\mathbf{x}_c - \boldsymbol{\omega}^{\mathrm{T}}\boldsymbol{\beta}(\mathbf{u})\mathbf{u} \tag{29}$$

$$= -\dot{\mathbf{q}}^{\mathrm{T}}\mathbf{D}\dot{\mathbf{q}} - \frac{1}{2}\mathbf{x}_c^{\mathrm{T}}\mathbf{Q}_c\mathbf{x}_c. \tag{30}$$

The closed-loop system is stable, since $\dot{V}_1$ is negative semidefinite. The restriction on the initial condition ensures that $V_1(\mathbf{q}, \dot{\mathbf{q}}, \mathbf{x}_c) \leq V_1(\mathbf{q}(0), \dot{\mathbf{q}}(0), \mathbf{x}_c(0)) < \Sigma_{i=1}^{n} 2k_{p,i}$, which guarantees that the Gibbs parameters do not reach a singularity. Due to the fact that $\mathbf{Q}_c = \mathbf{Q}_c^{\mathrm{T}} > 0$, $\dot{V}_1 = 0$ only if $\sqrt{\mathbf{D}}\dot{\mathbf{q}} = \mathbf{0}$ and $\mathbf{x}_c = \mathbf{0}$, which in turn implies that $\dot{\mathbf{x}}_c = \mathbf{0}$. Substituting these values into Eqs. (16) and (17) gives $\mathbf{B}_c\hat{\mathbf{y}} = \mathbf{0}$ and $\mathbf{u} = \mathbf{0}$. Owing to the fact that $\mathbf{B}_c$ has full column rank, it can be concluded that $\hat{\mathbf{y}} = \boldsymbol{\beta}(\mathbf{u})\boldsymbol{\omega} = \mathbf{0}$. Given that $\mathbf{u} = \mathbf{0}$, it is known that $\boldsymbol{\beta}(\mathbf{u}) \neq \mathbf{0}$, which in turn implies that $\boldsymbol{\omega} = \mathbf{0}$. Employing the zero-rate detectability assumption, it is known that $\sqrt{\mathbf{D}}\dot{\mathbf{q}} = \mathbf{0}$ and $\boldsymbol{\omega} = \mathbf{0}$, which implies that $\dot{\mathbf{q}} = \ddot{\mathbf{q}} = \mathbf{0}$. Substituting $\dot{\mathbf{q}} = \ddot{\mathbf{q}} = \mathbf{0}$ into Eq. (10), it can be shown that $\mathbf{q} = \mathbf{0}$. From LaSalle's Invariance Set Theorem it follows that the equilibrium point $(\mathbf{q}, \dot{\mathbf{q}}, \mathbf{x}_c) = (\mathbf{0}, \mathbf{0}, \mathbf{0})$ is asymptotically stable.[32] Therefore, $(\mathbf{q}, \dot{\mathbf{q}}, \mathbf{x}_c) \to (\mathbf{0}, \mathbf{0}, \mathbf{0})$ as $t \to \infty$. □

Theorem 2. The dynamics of the multi-link flexible-joint manipulator found in Eq. (10) on the domain $-\pi < \theta_i < \pi, -\pi < \alpha_i < \pi, \dot{\theta}_i \in \mathbb{R}, \dot{\alpha}_i \in \mathbb{R},\ i = 1, 2, \ldots, n$ together with the control law given by Eq. (21) render the equilibrium point $(\mathbf{q}, \dot{\mathbf{q}}, \mathbf{x}_c) = (\mathbf{0}, \mathbf{0}, \mathbf{0})$ of the closed-loop system asymptotically stable if

$$V_2(\mathbf{q}(0), \dot{\mathbf{q}}(0), \mathbf{x}_c(0)) = \frac{1}{2}\dot{\mathbf{q}}^{\mathrm{T}}(0)\mathbf{M}\dot{\mathbf{q}}(0) + \frac{1}{2}\mathbf{q}^{\mathrm{T}}(0)\mathbf{K}\mathbf{q}(0) + \frac{1}{2}\mathbf{x}_c^{\mathrm{T}}(0)\mathbf{P}_c\mathbf{x}_c(0) + \sum_{i=1}^{n} 2k_{p,i}\left(\sqrt{1+(\theta_i(0)/2)^2} - 1\right) < \sum_{i=1}^{n} 2k_{p,i}\left(\sqrt{1+\pi^2/4} - 1\right). \tag{31}$$

https://doi.org/10.1017/S0263574714002343 Published online by Cambridge University Press

Proof. Once again it can be easily shown using Eq. (10) and Eq. (21) that $(\mathbf{q}, \dot{\mathbf{q}}, \mathbf{x}_c) = (\mathbf{0}, \mathbf{0}, \mathbf{0})$ is in fact an equilibrium point of the closed-loop system. Let

$$\boldsymbol{\tau} = \mathbf{u}_p + \boldsymbol{\sigma}(\mathbf{u}) = -\mathbf{K}_p \begin{bmatrix} f(\theta_1/2) \\ f(\theta_2/2) \\ \vdots \\ f(\theta_n/2) \end{bmatrix} + \boldsymbol{\sigma}(\mathbf{u}), \tag{32}$$

where $f(\theta_i/2) = (\theta_i/2)/\sqrt{1 + (\theta_i/2)^2}$, $i = 1, 2, \ldots, n$. Now, consider the following Lyapunov function candidate,

$$V_2(\mathbf{q}, \dot{\mathbf{q}}, \mathbf{x}_c) = \frac{1}{2}\dot{\mathbf{q}}^{\mathrm{T}}\mathbf{M}\dot{\mathbf{q}} + \frac{1}{2}\mathbf{q}^{\mathrm{T}}\mathbf{K}\mathbf{q} + \sum_{i=1}^{n} 2k_{p,i}\left(\sqrt{1 + (\theta_i/2)^2} - 1\right) + \frac{1}{2}\mathbf{x}_c^{\mathrm{T}}\mathbf{P}_c\mathbf{x}_c. \tag{33}$$

Taking the derivative of V_2 with respect to time, simplifying using Eq. (10) and $\omega_i = \dot{\theta}_i$, $i = 1, 2, \ldots, n$, and following a similar procedure to the proof of Theorem 1 gives

$$\dot{V}_2 = -\dot{\mathbf{q}}^{\mathrm{T}}\mathbf{D}\dot{\mathbf{q}} - \frac{1}{2}\mathbf{x}_c^{\mathrm{T}}\mathbf{Q}_c\mathbf{x}_c. \tag{34}$$

The closed-loop system is stable, since $\dot{V}_2$ is negative semidefinite. The restriction on the initial condition ensures that $V_2(\mathbf{q}, \dot{\mathbf{q}}, \mathbf{x}_c) \leq V_2(\mathbf{q}(0), \dot{\mathbf{q}}(0), \mathbf{x}_c(0)) < \Sigma_{i=1}^{n} 2k_{p,i}(\sqrt{1 + \pi^2/4} - 1)$, which guarantees that $-\pi < \theta_i(t) < \pi$, $i = 1, 2, \ldots, n$, $\forall t \in \mathbb{R}^+$ and unwinding is avoided. Due to the fact that $\mathbf{Q}_c = \mathbf{Q}_c^{\mathrm{T}} > 0$, $\dot{V}_2 = 0$ only if $\sqrt{\mathbf{D}}\dot{\mathbf{q}} = \mathbf{0}$ and $\mathbf{x}_c = \mathbf{0}$, which in turn implies that $\dot{\mathbf{x}}_c = \mathbf{0}$. Substituting these values into Eqs. (16) and (17) gives $\mathbf{B}_c\hat{\mathbf{y}} = \mathbf{0}$ and $\mathbf{u} = \mathbf{0}$. Owing to the fact that $\mathbf{B}_c$ has full column rank, it can be concluded that $\hat{\mathbf{y}} = \boldsymbol{\beta}(\mathbf{u})\boldsymbol{\omega} = \mathbf{0}$. Given that $\mathbf{u} = \mathbf{0}$, it is known that $\boldsymbol{\beta}(\mathbf{u}) \neq \mathbf{0}$, which in turn implies that $\boldsymbol{\omega} = \mathbf{0}$. Employing the zero-rate detectability assumption, it is known that $\sqrt{\mathbf{D}}\dot{\mathbf{q}} = \mathbf{0}$ and $\boldsymbol{\omega} = \mathbf{0}$, which implies that $\dot{\mathbf{q}} = \ddot{\mathbf{q}} = \mathbf{0}$. Substituting $\dot{\mathbf{q}} = \ddot{\mathbf{q}} = \mathbf{0}$ into Eq. (10), it can be shown that $\mathbf{q} = \mathbf{0}$. From LaSalle's Invariance Set Theorem it follows that the equilibrium point $(\mathbf{q}, \dot{\mathbf{q}}, \mathbf{x}_c) = (\mathbf{0}, \mathbf{0}, \mathbf{0})$ is asymptotically stable.[32] Therefore, $(\mathbf{q}, \dot{\mathbf{q}}, \mathbf{x}_c) \to (\mathbf{0}, \mathbf{0}, \mathbf{0})$ as $t \to \infty$. □

Notice that the closed-loop stability results only depend on the zero-rate detectability assumption. The numerical values of the mass, stiffness, and damping matrices do not influence the results, and as such, the closed-loop stability of the system is robust to modeling errors. The allowable set of initial conditions is a crucial part of the stability analysis, as it guarantees the avoidance of singularities and unwinding, and represents the region of attraction. The set of initial conditions can be physically interpreted as a requirement that the total initial energy of the system be low enough that the controller is able to regulate the system to the desired equilibrium point before a singularity is reached or unwinding occurs. For example, if a joint angle is very close to 180°, then assuming that the initial state of the controller is $\mathbf{x}_c(0) = \mathbf{0}$, the joint must not have an initial angular velocity that will cause it to surpass 180°. The region of attraction when using the control law of Eq. (20) is $\Omega_1 = \{\mathbf{q} \in \mathbb{R}^{2n}, \dot{\mathbf{q}} \in \mathbb{R}^{2n}, \mathbf{x}_c \in \mathbb{R}^{4n} \mid V_1(\mathbf{q}, \dot{\mathbf{q}}, \mathbf{x}_c) < \Sigma_{i=1}^{n} 2k_{p,i}\}$. The region of attraction when using the control law of Eq. (21) is $\Omega_2 = \{\mathbf{q} \in \mathbb{R}^{2n}, \dot{\mathbf{q}} \in \mathbb{R}^{2n}, \mathbf{x}_c \in \mathbb{R}^{4n} \mid V_2(\mathbf{q}, \dot{\mathbf{q}}, \mathbf{x}_c) < \Sigma_{i=1}^{n} 2k_{p,i}(\sqrt{1 + \pi^2/4} - 1) \approx 0.8621\Sigma_{i=1}^{n} 2k_{p,i}\}$. Although the Lyapunov functions V_1 and V_2 are different, by setting $\theta_i = p_i = 0$, $i = 1, \ldots, n$ they become identical and the region of attraction of Ω_1 is clearly larger than Ω_2. This increased region of attraction further motivates the use of the Gibbs parameter as a control variable in Eq. (20).

4.3. Controller synthesis

The synthesis of the SPR controller is accomplished by linearizing the equations of motion of the manipulator about the desired operating point including the proportional control precompensation term and using a Linear Quadratic Regulator (LQR) formulation along with the KYP Lemma. To linearize the equations of motion the term $\mathbf{f}_{non}$ is set to zero, all other parameters are evaluated at the desired equilibrium point and the proportional control term is included in the equation of motion.

https://doi.org/10.1017/S0263574714002343 Published online by Cambridge University Press

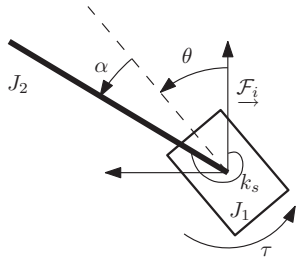


Fig. 5. Schematic of a flexible-joint.

The linearized system can then be written in a LTI state-space form:

$$\begin{bmatrix}\dot{\mathbf{q}}\\ \ddot{\mathbf{q}}\end{bmatrix} = \underbrace{\begin{bmatrix}\mathbf{0} & \mathbf{1}\\ -\mathbf{M}^{-1}(\mathbf{K}+\mathbf{K}_p) & -\mathbf{M}^{-1}\mathbf{D}\end{bmatrix}}_{\mathbf{A}_p}\underbrace{\begin{bmatrix}\mathbf{q}\\ \dot{\mathbf{q}}\end{bmatrix}}_{\mathbf{x}_p} + \underbrace{\begin{bmatrix}\mathbf{0}\\ \mathbf{M}^{-1}\hat{\mathbf{B}}\end{bmatrix}}_{\mathbf{B}_p}\boldsymbol{\sigma}(\mathbf{u}), \tag{35}$$

$$\mathbf{y} = \underbrace{\begin{bmatrix}\mathbf{0} & \mathbf{1}\end{bmatrix}}_{\mathbf{C}_p}\begin{bmatrix}\mathbf{q}\\ \dot{\mathbf{q}}\end{bmatrix}. \tag{36}$$

The SPR controller $(\mathbf{A}_c, \mathbf{B}_c, \mathbf{C}_c)$ can now be synthesized by following the method outlined in ref. [22]. This is done by first using the LQR formulation to find $\mathbf{C}_c = \mathbf{R}^{-1}\mathbf{B}_p^{\mathrm{T}}\mathbf{P}$ given weights $\mathbf{Q}$ and $\mathbf{R}$, where the matrix $\mathbf{P} = \mathbf{P}^{\mathrm{T}} > 0$ is the solution to the algebraic Riccati equation $\mathbf{P}\mathbf{A}_p + \mathbf{A}_p^{\mathrm{T}}\mathbf{P} - \mathbf{P}\mathbf{B}_p\mathbf{R}^{-1}\mathbf{B}_p^{\mathrm{T}}\mathbf{P} + \mathbf{Q} = \mathbf{0}$. Finally, the KYP Lemma is solved by choosing $\mathbf{Q}_c$ and solving for $\mathbf{P}_c$ to find $\mathbf{B}_c = \mathbf{P}_c^{-1}\mathbf{C}_c^{\mathrm{T}}$. The resulting controller $(\mathbf{A}_c, \mathbf{B}_c, \mathbf{C}_c)$ is now SPR, where $\mathbf{A}_c = \mathbf{A}_p - \mathbf{B}_p\mathbf{C}_c$.

5. Single-Link Manipulator Example

5.1. Single-link manipulator dynamics and control laws

A single-link flexible-joint manipulator, shown in Fig. 5 is an example of a flexible-joint manipulator with $n = 1$ links. The equations of motion of this system reduce to

$$\mathbf{M}\ddot{\mathbf{q}} + \mathbf{D}\dot{\mathbf{q}} + \mathbf{K}\mathbf{q} = \hat{\mathbf{b}}\tau_c. \tag{37}$$

Notice that in the case of the single-link manipulator the nonlinear term vanishes.

The control laws from Eqs. (20) and (21) can be simplified to

$$\tau = -k_p f(p) + \sigma(u), \tag{38}$$

$$\tau = -k_p f(\theta/2) + \sigma(u), \tag{39}$$

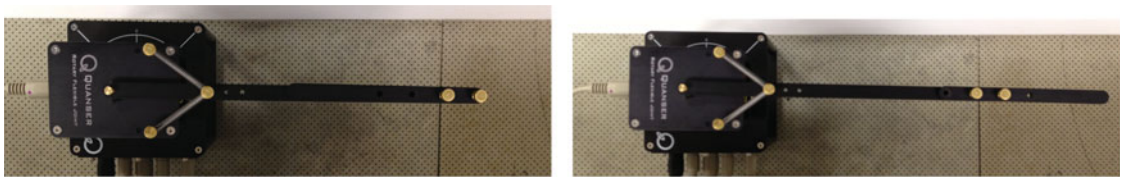
where $p = \tan(\theta/2)$, $\dot{\mathbf{x}}_c = \mathbf{A}_c\mathbf{x}_c + \mathbf{B}_c\beta(u)\dot{\theta}$, $-u = y_c = \mathbf{C}_c\mathbf{x}_c$, $\sigma(u) = \beta(u)u$, and the matrices $\mathbf{A}_c$, $\mathbf{B}_c$, and $\mathbf{C}_c$ are synthesized with weights $\mathbf{Q}$, R, and $\mathbf{Q}_c$ using the synthesis method outlined in Section 4.3.

5.2. Experimental results

The control laws from Eqs. (38) and (39) are experimentally tested on a rotary flexible-joint experimental testbed built by Quanser Consulting Inc.,[33] shown in Fig. 6.

The testbed has a hub second moment of mass of $J_1 = 2.08 \times 10^{-3}$ (kg·m^2), a link second moment of mass of $J_2 = 3.28 \times 10^{-3}$ (kg·m^2), a joint stiffness of $k_s = 1.3$ (N·m/rad), a hub damping coefficient of $d_1 = 4 \times 10^{-3}$ (N·m/(rad/s)), and a link damping coefficient of $d_2 = 1 \times 10^{-6}$ (N·m/(rad/s)). The base of the flexible joint is fixed, while the hub and link are rotated by an angle θ and α respectively. The performances of the two proposed control laws are compared to the performances

https://doi.org/10.1017/S0263574714002343 Published online by Cambridge University Press



(a) (b)

Fig. 6. (a) Nominal experimental system and (b) experimental system with link inertia perturbed to a value 22% greater than the nominal system.

of two existing controls designed to avoid actuator saturation in ref. [8]:

$$\tau = -k_p f(p) - k_d f(\omega), \tag{40}$$

$$\tau = -k_p f(\theta/2) - k_d f(\omega). \tag{41}$$

All experiments are performed on the system with a perturbed link inertia, as shown in Fig. 6. The SPR controller is synthesized for the nominal system, but implemented to control the perturbed system, which has a link second moment of mass that is approximately 22% greater than that of the nominal system.

An initial attitude of $\theta = -90^\circ$ and $\alpha = 0^\circ$ is used along with an initial angular velocity of $\dot{\theta} = \dot{\alpha} = 0^\circ/s$. The desired equilibrium attitude is $\theta_d = \alpha_d = 0^\circ$. For these tests $k_p = 0.6$ (N·m) and $\bar{u} = 0.15$ (N·m), which guarantees $|\tau| \leq 0.75$ (N·m). The control gains for Eqs. (40) and (41) are set to $k_p = 0.6$ (N·m) and $k_d = 0.15$ (N·m) to guarantee the same maximum torque. The SPR controller is synthesized with $\mathbf{Q} = \text{diag}\{1,\ 1,\ 10,\ 10\}$, $R = 0.4$, and $\mathbf{Q}_c = \text{diag}\{100,\ 100,\ 1000,\ 1000\}$. In Fig. 7 are the θ, α, $\omega = \dot{\theta}$, u_p, u_d, u, τ, and β responses versus time for all controllers.

The experimental results show that closed-loop asymptotic stability about a desired set point can be achieved using the proposed controllers, even in the presence of a significant model perturbation. As seen in Fig. 7(h), the derivative control clearly exceeds the saturation limit, triggering $\beta \neq 1$ and avoiding actuator saturation, as shown in Fig. 7(d). In Fig. 7(a) a certain amount of overshoot is present in all responses of θ. The proportional control effort is clearly higher when using the function $f(p)$ instead of $f(\theta/2)$ in the control law, which reduces the rise time of θ. In applications where any overshoot is unacceptable, the value assigned to k_p could be lowered and the value assigned to $\bar{u}$ could be raised, so that the derivative control becomes more dominant while maintaining the same actuator saturation limit of $|\tau| \leq k_p + \bar{u}$. It is also observed in Fig. 7(d) that the control laws of Eqs. (40) and (41) result in noisier derivative control compared to the control laws of Eqs. (38) and (39). This is explained by the dynamic nature of the SPR controller, whose gain rolls off at high frequency, which is the key benefit of the proposed controllers. Note that any steady-state error in the experimental results is due to the unmodeled static friction in the testbed. In practice, a friction compensator could be developed to overcome this issue.

6. Two-Link Manipulator Example

Consider a flexible-joint manipulator with two links ($n = 2$). The equations of motion of the system are defined in Eq. (10). The control laws in Eqs. (20) and (21) are implemented in a simulation of a two-link flexible-joint manipulator as

$$\boldsymbol{\tau} = -\mathbf{K}_p \mathbf{f}(\mathbf{p}) + \boldsymbol{\sigma}(\mathbf{u}), \tag{42}$$

$$\boldsymbol{\tau} = -\mathbf{K}_p \mathbf{f}(\boldsymbol{\theta}/2) + \boldsymbol{\sigma}(\mathbf{u}), \tag{43}$$

where $\mathbf{p} = [\tan(\theta_1/2) \quad \tan(\theta_2/2)]^{\mathrm{T}}$, $\dot{\mathbf{x}}_c = \mathbf{A}_c \mathbf{x}_c + \mathbf{B}_c \boldsymbol{\beta}(\mathbf{u})\dot{\boldsymbol{\theta}}$, $-\mathbf{u} = \mathbf{y}_c = \mathbf{C}_c \mathbf{x}_c$, $\boldsymbol{\sigma}(\mathbf{u}) = \boldsymbol{\beta}(\mathbf{u})\mathbf{u}$, and the matrices $\mathbf{A}_c$, $\mathbf{B}_c$, and $\mathbf{C}_c$ are synthesized with weights $\mathbf{Q}$, $\mathbf{R}$, and $\mathbf{Q}_c$ using the synthesis method outlined in Section 4.3. The numerical properties of the manipulator are presented in Table I. Note that J_3 and J_4 are the second moment of masses of the second link and second hub respectively, $\mathbf{c}_4$ is the first moment of mass of the second link, l_2 and l_4 are the lengths of the first and second link

https://doi.org/10.1017/S0263574714002343 Published online by Cambridge University Press

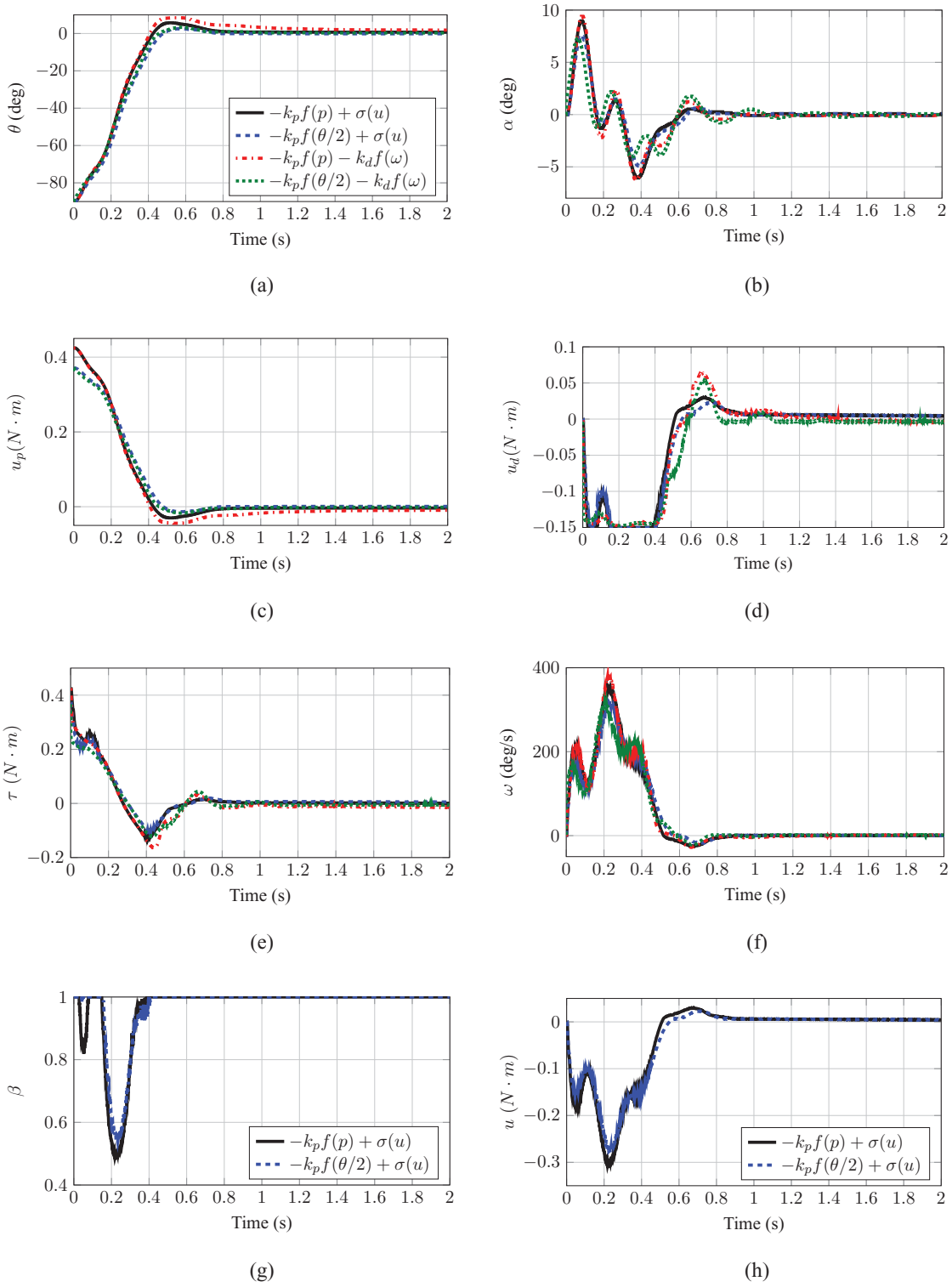


Fig. 7. Single-link system experimental results: (a) θ vs. time, (b) α vs. time, (c) u_p vs. time, (d) $\sigma(u_d)$ vs. time, (e) τ vs. time, (f) ω vs. time, (g) β vs. time, and (h) u vs. time. Plots (b)–(f) use the same legend as plot (a). Note the noise present in the derivative control effort in (d) when using the control laws from ref. [8], which is clearly not present with the control laws in Eqs. (38) and (39).

https://doi.org/10.1017/S0263574714002343 Published online by Cambridge University Press

Table I. Physical properties of the two-link flexible-joint manipulator.

Property	**Value**	**Units**
$J_1,\ J_3$	$2.08 \cdot 10^{-3}$	kg·m^2
$J_2,\ J_4$	$3.28 \cdot 10^{-3}$	kg·m^2
l_2	0.298	m
m_2	0.094	kg
m_3	0.5	kg
m_p	0.1	kg
m_4	0.094	kg
l_4	0.250	m
$\mathbf{c}_4$	$[0\ 0.0243\ 0]^{\mathrm{T}}$	kg·m
$k_{s,1}$	1.1	N·m/rad
$k_{s,2}$	1.3	N·m/rad
$d_1,\ d_3$	$4 \cdot 10^{-3}$	N·m/(rad/s)
$d_2,\ d_4$	$1 \cdot 10^{-6}$	N·m/(rad/s)

respectively, m_2 is the mass of the first link, m_3 and m_4 are the masses of the second hub and link respectively, d_3 and d_4 are the damping coefficients of the second hub and link respectively, and $k_{s,1}$ and $k_{s,2}$ are the torsional stiffness constants of the first and second joint respectively. The symbols that were used in Section 5 represent the same system properties.

Similarly to the single-link manipulator experiments, the performances of the two proposed controllers are compared to the performances of two saturation avoidance controllers in ref. [8]:

$$\boldsymbol{\tau} = -\mathbf{K}_p \mathbf{f}(\mathbf{p}) - \mathbf{K}_d \mathbf{f}(\boldsymbol{\omega}), \tag{44}$$

$$\boldsymbol{\tau} = -\mathbf{K}_p \mathbf{f}(\boldsymbol{\theta}/2) - \mathbf{K}_d \mathbf{f}(\boldsymbol{\omega}), \tag{45}$$

where $\mathbf{K}_d = \mathrm{diag}\{k_{d,1}, k_{d,2}\}$, $0 < k_{d,1} < \infty$, and $0 < k_{d,2} < \infty$.

For the simulation, the initial angular velocities are set to $\omega_1 = 0^\circ/\mathrm{s}$ and $\omega_2 = 0^\circ/\mathrm{s}$, while the initial attitude is set to $\theta_1 = -90^\circ$, $\theta_2 = -15^\circ$, and $\alpha_1 = 0^\circ = \alpha_2 = 0^\circ$. The desired equilibrium point is $\theta_{1,d} = \theta_{2,d} = \alpha_{1,d} = \alpha_{2,d} = 0^\circ$. The control gains used with the control laws of Eqs. (20) and (21) are $k_{p,1} = 0.9$ (N·m), $k_{p,2} = 0.7$ (N·m), $\bar{u}_1 = 0.15$ (N·m), and $\bar{u}_2 = 0.1$ (N·m), which guarantees $|\tau_1| \leq 1.05$ (N·m) and $|\tau_2| \leq 0.8$ (N·m). Similarly, the control gains used with the control laws of Eqs. (44) and (45) are $k_{p,1} = 0.9$ (N·m), $k_{p,2} = 0.7$ (N·m), $k_{d,1} = 0.15$ (N·m), and $k_{d,2} = 0.1$ (N·m), which also guarantees $|\tau_1| \leq 1.05$ (N·m) and $|\tau_2| \leq 0.8$ (N·m). The saturation limit of each actuator is set differently to emphasize the fact that the saturation limits can be chosen independently for each actuator. The SPR controller is synthesized with $\mathbf{Q} = \mathrm{diag}\{1, 1, 1, 1, 10, 10, 10, 10\}$, $\mathbf{R} = \mathrm{diag}\{0.1, 0.1\}$, and $\mathbf{Q}_c = \mathrm{diag}\{100, 100, 100, 100, 1000, 1000, 1000, 1000\}$. Measurement noise is added to the angular velocity measurement as $\omega_1 = \dot{\theta}_1 + 0.01 \sin(10^6 t)$ and $\omega_2 = \dot{\theta}_2 + 0.01 \sin(10^6 t + \pi/3)$, in order to simulate measurements from an imperfect sensor. The response of $\theta_1, \theta_2, \alpha_1, \alpha_2, \omega_1, \omega_2$, as well as $u_{p,1}, u_{p,2}, u_{d,2}, u_{d,2}, u_1, u_2, \tau_1, \tau_2, \beta_1$, and β_2 can be found in Figs. 8 and 9.

The results of the two-link manipulator simulation are quite similar to those found in the single-link manipulator experiments. Although the nonlinear derivative control of the first and second actuators experience significant saturation, asymptotic stability is achieved about the desired set point. The derivative control effort applied when using the control laws from ref. [8] experiences a significant amount of noise, as seen in Figs. 8(d) and 9(d). Although this does not have a noticeable impact on the set-point regulation of the joint angles, in practice the actuators of the manipulator will most likely not be able to handle the extremely high frequencies associated with the control torque demanded by the control law. The derivative control when using the Hammerstein SPR derivative control in Eqs. (20) and (21) is quite smooth in Figs. 8(d) and 8(d), since the controller is designed for its gain to roll off at high frequency. This highlights the main benefit of the proposed control laws. Once again, overshoot in θ_1 and θ_2 is present in Figs. 8(a) and 9(a), which can be tuned by modifying the values of $k_{p,i}$ and $\bar{u}_i$ as mentioned previously.

https://doi.org/10.1017/S0263574714002343 Published online by Cambridge University Press

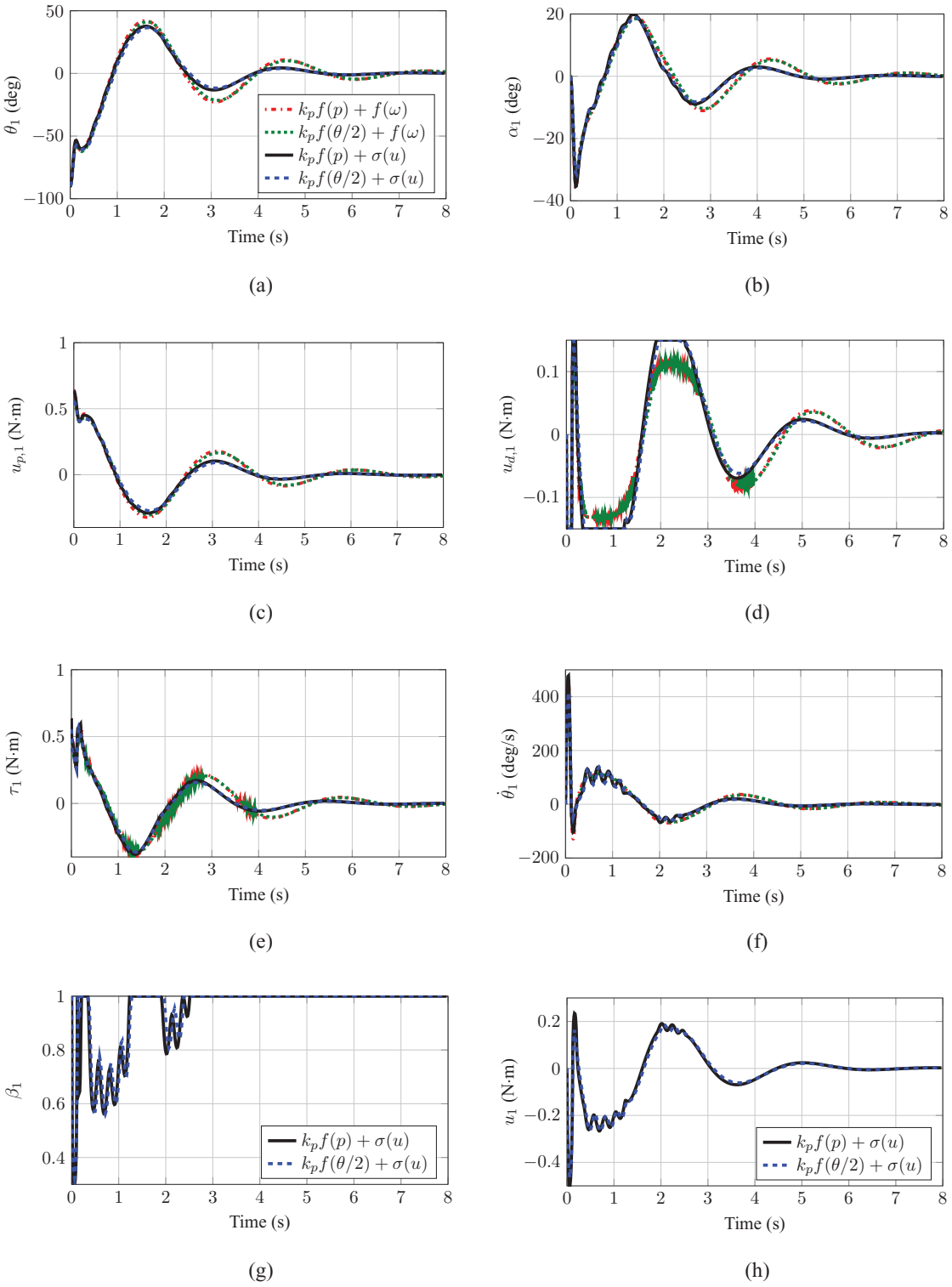


Fig. 8. Two-link manipulator simulation results: (a) θ_1 vs. time, (b) α_1 vs. time, (c) $u_{p,1}$ vs. time, (d) $\sigma_1(u_{d,1})$ vs. time, and (e) β_1 vs. time. Plots (b)–(e) use the same legend as plot (a). Note that a significant amount of noise is present in the derivative control effort of (d) and the applied torque of (e) when using the control laws from ref. [8]. The proposed control laws of Eqs. (20) and (21) are able to filter out the measurement noise, as seen in (d) and (e).

https://doi.org/10.1017/S0263574714002343 Published online by Cambridge University Press

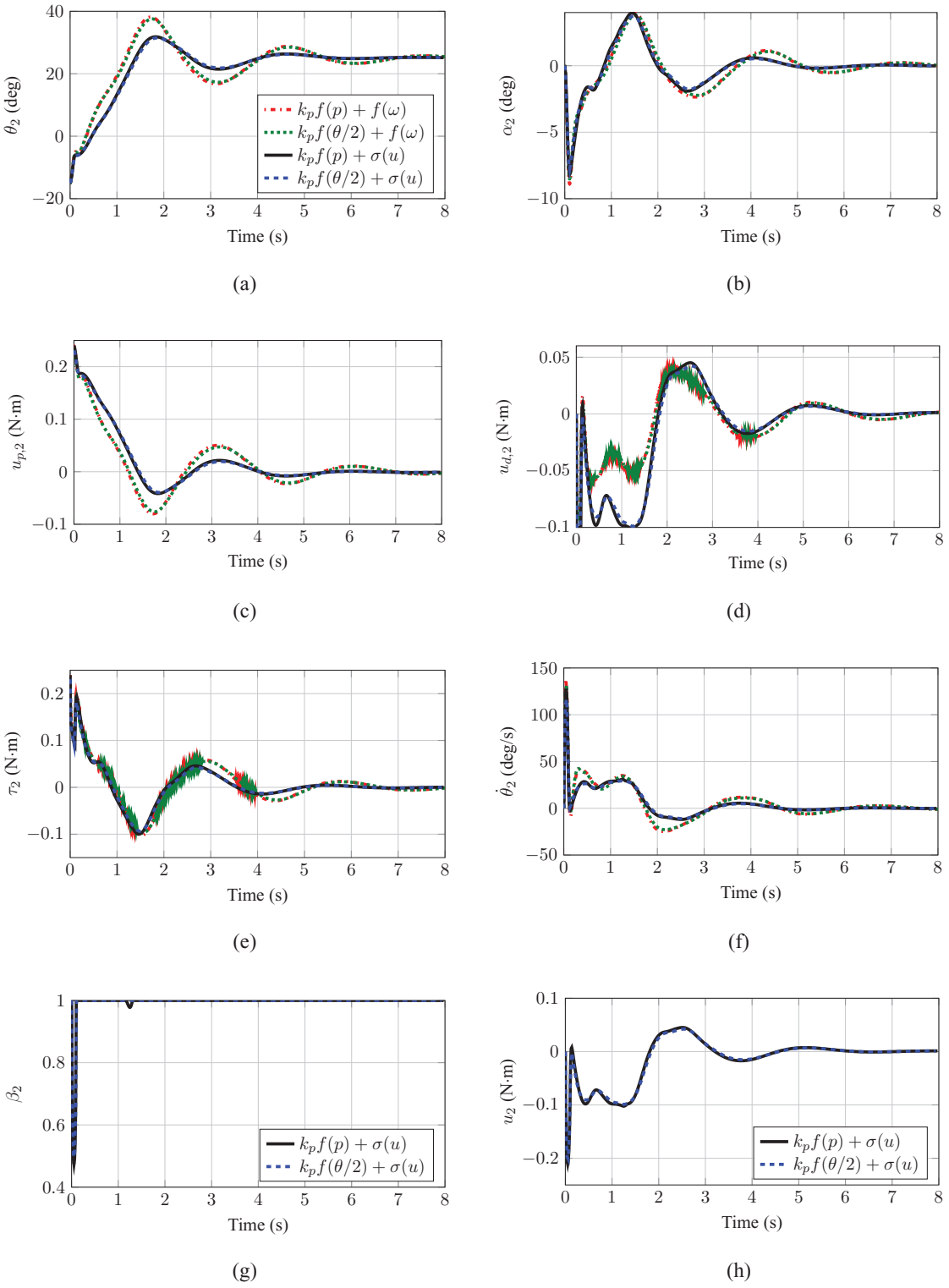


Fig. 9. Two-link manipulator simulation results: (a) θ_2 vs. time, (b) α_2 vs. time, (c) $u_{p,2}$ vs. time, (d) $\sigma_2(u_{d,2})$ vs. time, and (e) β_2 vs. time. Plots (b)–(e) use the same legend as plot (a). Note that a significant amount of noise is present in the derivative control effort of (d) and the applied torque of (e) when using the control laws from ref. [8]. The proposed control laws of Eqs. (20) and (21) are able to filter out the measurement noise, as seen in (d) and (e).

https://doi.org/10.1017/S0263574714002343 Published online by Cambridge University Press

7. Conclusion

The saturated controllers presented in this paper avoid saturation by using a bounded proportional control term from ref. [8] and a Hammerstein SPR rate controller. This control architecture guarantees that the total torque demanded from each actuator remains below the maximum torque that each actuator can provide. Restrictions are placed on the allowable set of initial conditions in order to ensure the asymptotic stability of the closed-loop system. Without these restrictions, the Gibbs parameter may approach a singularity or the system may experience unwinding. Experimental and simulation results suggest that the proposed controllers perform well even in the presence of significant controller saturation and measurement noise. In particular, the simulation results highlight the fact that the Hammerstein SPR rate controller can filter out measurement noise at high frequencies, which the control laws from ref. [8] are not capable of.

References

1. S. D. Eppinger and W. P. Seering, "Three dynamic problems in robot force control," *IEEE Trans. Robot. Autom.* **8**(6), 751–758 (1992).
2. E. I. Rivin, *Mechanical Design of Robots* (Mcgraw-Hill, 1987).
3. R. Ortega, R. Kelly and A. Loría, "A class of output feedback globally stabilizing controllers for flexible joints robots," *IEEE Trans. Robot. Autom.* **11**(5), 766–770 (1995).
4. S. Ulrich and J. Z. Sasiadek, "Modeling and direct adaptive control of a flexible-joint manipulator," *J. Guid. Control Dyn.* **35**(1), 25–39 (2012).
5. P. Tomei, "A simple PD controller for robots with elastic joints," *IEEE Trans. Autom. Control* **36**(20), 1208–1213 (1991).
6. R. Ortega, A. Loría, P. J. Nicklasson and H. J. Sira-Ramirez, *Passivity-Based Control of Euler-Lagrange Systems* (Springer, 1998).
7. M. W. Spong, "Modeling and control of elastic joint robots," *J. Dyn. Syst. Meas. Control* **109**(4), 310–319 (1987).
8. R. J. Caverly, D. E. Zlotnik, L. J. Bridgeman and J. R. Forbes, "Saturated proportional derivative control of flexible-joint manipulators," *Robot. Comput.-Integr. Manuf.* **30**(6), 658–666 (2014).
9. A. Aldu-Schäffer, C. Ott and G. Hirzinger, "A unified passivity-based framework for position, torque and impedance control of flexible joint robots," *Int. J. Robot. Res.* **26**(1), 23–39 (2007).
10. W. E. Dixon, E. Zergeroglu, D. M. Dawson and M. W. Hannan, "Global adaptive partial state feedback tracking control of rigid-link flexible-joint robots," *Robotica* **18**(3), 324–336 (2000).
11. R. Lozano and B. Brogliato, "Adaptive control of robot manipulators with flexible joints," *IEEE Trans. Autom. Control* **37**(2), 174–181 (1992).
12. M. W. Spong, K. Khorasani and P. V. Kokotovic, "An integral manifold approach to the feedback control of flexible joint robots," *IEEE J. Robot. Autom.* **3**(4), 291–300 (1987).
13. C. J. B. Macnab and G. M. T. D'Eleuterio, "Neuroadaptive control of elastic-joint robots using robust performance enhancement," *Robotica* **19**(6), 619–629 (2001).
14. A. Ailon and R. Ortega, "An observer-based set-point controller for robot manipulators with flexible joints," *Syst. Control Lett.* **21**, 329–335 (1993).
15. D. S. Bernstein and A. N. Michel, "A chronological bibliography on saturating actuators," *Int. J. Robust Nonlinear Control* **5**, 375–380 (1995).
16. H. Liu, S. Zhu and Z. Chen, "Saturated output feedback tracking control for robot manipulators via fuzzy self-tuning," *J. Zhejiang Univ. Sci. C (Comput. Electron.)* **11**(12), 956–966 (2010).
17. J. Moreno-Valenzuela and V. Santibáñez, "Robust saturated PI joint velocity control for robot manipulators," *Asian J. Control* **15**(1), 64–79 (2013).
18. H. Arai, K. Tanie and S. Tachi, "Path tracking control of a manipulator considering torque saturation," *IEEE Trans. Ind. Electron.* **41**(1), 25–31 (1994).
19. V. M. Hernández-Guzmán, V. Santibanez and A. Zavala-Río, "A saturated PD controller for robots equipped with brushless DC-motors," *Robotica* **28**(3), 405–411 (2009).
20. D. S. Bernstein and W. M. Haddad, "Nonlinear controllers for positive real systems with arbitrary input nonlinearities," *IEEE Trans. Autom. Control* **39**(7), 1513–1517 (1994).
21. W. M. Haddad and V. Chellaboina, "Nonlinear control of Hammerstein systems with passive nonlinear dynamics," *IEEE Trans. Autom. Control* **46**(10), 1630–1634 (2001).
22. R. J. Benhabib, R. P. Iwens and R. L. Jackson, "Stability of large space structure control systems using positivity concepts," *J. Guid. Control* **4**, 487–494 (Sept.–Oct. 1981).
23. P. C. Hughes, *Spacecraft Attitude Dynamics*, 2nd ed. (Mineola, New York, Dover, 2004).
24. H. Marquez, *Nonlinear Control Systems* (Hoboken, NJ, John Wiley and Sons, Inc., 2003).
25. M. W. Spong, S. Hutchinson and M. Vidyasagar, *Robot Modeling and Control*, 1st ed. (Wiley, 2005).
26. Y. Su and C. Zheng, "Globally asymptotic stabilization of spacecraft with simple saturated proportional-derivative control," *J. Guid. Control Dyn.* **34**(6), 1932–1935 (2011).
27. S. P. Bhat and D. S. Bernstein, "A topological obstruction to continuous globabl stabilization of rotational motion and the unwinding phenomenon," *Syst. Control Lett.* **39**, 63–70 (2000).

https://doi.org/10.1017/S0263574714002343 Published online by Cambridge University Press

28. T. Lee, "Exponential stability of an attitude tracking control system on SO(3) for large-angle rotation maneuvers," *Syst. Control Lett.* **61** 231–237 (2012).
29. O. Egeland and J. M. Godhavn, "Passivity-based adaptive attitude control of a rigid spacecraft," *IEEE Trans. Autom. Control* **39**(4), 842–846 (1994).
30. C. J. Damaren, "Gain scheduled SPR controllers for nonlinear flexible systems," *J. Dyn. Syst. Meas. Control* **118**(4), 698–703 (1996).
31. L. Lanari and J. T. Wen, "Asymptotically stable set point control laws for flexible robots," *Syst. Control Lett.* **19**, 119–129 (1992).
32. J. J. E. Slotine and W. Li, *Applied Nonlinear Control* (New Jersey, Prentice-Hall, 1991).
33. Quanser Consulting Inc., 2011. Quanser Rotary Servo User Manual.

https://doi.org/10.1017/S0263574714002343 Published online by Cambridge University Press